arXiv:1210.6138v1 [cond-mat.mes-hall] 23 Oct 2012

How to Directly Measure Kondo Cloud's Length

Jinhong Park,[1] S.-S. B. Lee,[1] Yuval Oreg,[2] and H.-S. Sim[1, *]
[1] *Department of Physics, Korea Advanced Institute of Science and Technology, Daejeon 305-701, Korea*
[2] *Department of Condensed Matter Physics, Weizmann Institute of Science, Rehovot 76100, Israel*

(Dated: October 24, 2012)

We propose a method to directly measure, by electrical means, the Kondo screening cloud formed by an Anderson impurity coupled to semi-infinite quantum wires, on which an electrostatic gate voltage is applied at distance L from the impurity. We show that the Kondo cloud, and hence the Kondo temperature and the electron conductance through the impurity, are affected by the gate voltage, as L decreases below the Kondo cloud length. Based on this behavior, the cloud length can be experimentally identified by changing L with a keyboard type of gate voltages or tuning the coupling strength between the impurity and the wires.

PACS numbers: 72.15.Qm,73.63.Kv,72.10.Fk

Introduction.— The Kondo effect is a central many-body problem of condensed matter physics [1, 2]. It involves a spin singlet, formed by the spin-spin interaction between a magnetic impurity and surrounding conduction electrons. Deeper understanding of the effect has been achieved by using a quantum dot, that hosts a magnetic impurity spin, under systematic control [3–6].

Although the Kondo effect is well known and widely studied, its spatial features still remain to be addressed. The Kondo spin singlet is formed below a certain energy scale, the Kondo temperature T_K. This implies that the singlet is formed over a spatially extended conduction-electron region of length scale $\xi_K = \hbar v_F/(k_B T_K)$, where v_F is the Fermi velocity. The region is called the Kondo screening cloud. When $T_K \sim 1$ K and $v_F \sim 10^5$-10^6 m/s, the cloud has the size of micrometers. There have been several proposals [7–19] for ways to detect the cloud.

Despite of the proposals, there has been no conclusive measurement supporting the existence of the Kondo cloud [20, 21]. The difficulty to detect the cloud arises because it is essentially a spin cloud. More than that, the conduction spin forming the Kondo spin singlet exhibits quantum fluctuations, resulting in zero averaged spin. A way of detecting the cloud is to study the spin-spin correlation [7–10] between the impurity and the conduction electrons. However it requires measurements of spin dynamics of time scale $\hbar/(k_B T_K)$. STM studies probing local density of states may be also useful [11–13]. Recent STM measurements [22–24] have progress, showing the signatures of the Kondo effect in the region away from a magnetic impurity, whose spatial extension is however much shorter than ξ_K. Another direction is to study a magnetic impurity in a finite-size system, using persistent current [14] or electron conductance [15–18]. In this case, because the cloud cannot extend beyond the finite size, the Kondo effect is strongly affected, and suppressed when the size is shorter than ξ_K. There has been no experimental report in this direction.

In this work, we propose a new way of detecting the Kondo cloud, based on the intuition that a change of conduction electrons inside the cloud will affect the Kondo effect. We consider a Kondo impurity formed in a quantum dot (at $x = 0$) coupled to two semi-infinite ballistic quantum wires with electron tunneling amplitude t_{WD} (see Fig. 1). Electrostatic gate voltages V_g are applied to the wires at distance L from the dot (in $|x| > L$), and modify *indirectly* the local density of states $\rho(\epsilon)$ of conduction electrons nearby the dot (see Fig. 2); our approach is applicable also when V_g is applied to only one wire. We find that when $L \gg \xi_K$, V_g does not affect the cloud. However, when $L \ll \xi_K$, the cloud, hence the Kondo temperature T_K and the electron conductance G of the dot, are sensitive to V_g. The crossover between the two regimes occurs at $L \approx \xi_K$. By measuring G or T_K with varying L or t_{WD} (see Figs. 3 and 4), one can detect the crossover and hence ξ_K. We remark that the cloud is extensible to $|x| > L$, hence, not suppressed even for $L \ll \xi_K$ in our approach; this is in contrast to the case [15–17] where the cloud is limited by the finite system size. We analyze the system using the poor man scaling [25], the numerical renormalization group (NRG) study [26–28], and the Fermi liquid theory [29].

The setup.— We describe the wires by the tight-

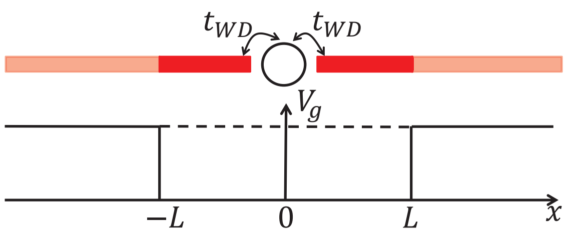

FIG. 1: (Color Online) Setup for detecting the Kondo cloud. A quantum dot located at $x = 0$ hosts a magnetic impurity spin. It couples to quantum wires along $\hat{x}$ axis, with electron tunneling amplitude t_{WD}. Gate voltage V_g is applied at distance L from the dot (in $|x| > L$). The Kondo effect becomes sensitive to V_g, as L decreases below the cloud length.

binding Hamiltonian with sites j's in wire $i = l, r$,

$$\begin{aligned} H_W &= \sum_{i=l,r} \sum_{j=1}^{\infty} \sum_{\sigma=\uparrow,\downarrow} [\epsilon_0 n_{ij\sigma} + (-t c_{ij\sigma}^\dagger c_{i(j+1)\sigma} + \text{H.c.})] \\ &\quad - eV_g \sum_{i=l,r} \sum_{j=N+1}^{\infty} \sum_{\sigma=\uparrow,\downarrow} n_{ij\sigma}, \end{aligned} \tag{1}$$

where $c_{ij\sigma}^\dagger$ creates an electron with spin σ and energy ϵ_0 at site j in wire i, $n_{ij\sigma} \equiv c_{ij\sigma}^\dagger c_{ij\sigma}$, and t is the hopping energy. The last term describes the gate voltage V_g applied to the two wires in $|x| > L = Na$, where a is the lattice spacing. $V_g(x)$ changes at $x = L$ abruptly over the length shorter than the Fermi wave length. The dot Hamiltonian H_D is modeled by the Anderson impurity [30], $H_D = \sum_{\sigma=\uparrow,\downarrow} \epsilon_d d_\sigma^\dagger d_\sigma + U n_{d\uparrow} n_{d\downarrow}$, where $d_\sigma^\dagger$ creates an electron with energy ϵ_d and spin σ in the dot, $n_{d\sigma} \equiv d_\sigma^\dagger d_\sigma$, and U is the electron repulsive interaction of the dot. $H_T = -t_{WD} \sum_i \sum_{\sigma=\uparrow,\downarrow} (c_{i1\sigma}^\dagger d_\sigma + \text{H.c.})$ describes electron tunneling between the wire and the dot.

The dot is occupied by a single electron in the Coulomb blockade regime of $\epsilon_d < \epsilon_F$ and $\Gamma(\epsilon_F) \ll -\epsilon_d + \epsilon_F$, $U + \epsilon_d - \epsilon_F$, where $\Gamma(\epsilon) = 2\pi |t_{WD}|^2 \rho(\epsilon)$ is the hybridization function between the dot and the wires (i.e., the level broadening), $\rho(\epsilon)$ is the local density of states at energy ϵ in the sites $j = 1$ (the neighboring sites of the dot) of the wires, and ϵ_F is the Fermi energy. In this regime, the total Hamiltonian of the setup is transformed by the Schrieffer-Wolf transformation into [2, 31]

$$H = H_D + H_W + H_T \simeq J \vec{s} \cdot \vec{S} + V \sum_{i,\sigma} n_{i1\sigma} + H_W. \tag{2}$$

Here, the Kondo impurity spin, $\vec{S} = \sum_{\sigma,\sigma'} d_\sigma^\dagger \vec{\sigma}_{\sigma\sigma'} d_{\sigma'}/2$, couples with the spin of the neighboring conduction electrons, $\vec{s} = \sum_{\sigma,\sigma'} (c_{l1\sigma}^\dagger + c_{r1\sigma}^\dagger) \vec{\sigma}_{\sigma\sigma'} (c_{l1\sigma'} + c_{r1\sigma'})/2$, with strength $J = 2t_{WD}^2[-1/(\epsilon_d - \epsilon_F) + 1/(U + \epsilon_d - \epsilon_F)]$. The second term describes the potential scattering with strength $V = t_{WD}^2[-1/(\epsilon_d - \epsilon_F) - 1/(U + \epsilon_d - \epsilon_F)]/2$.

Local density of states.— We show how the gate voltage V_g changes the local density of states $\rho(\epsilon)$ of conduction electrons near the impurity (at sites $j = 1$). We calculate $\rho(\epsilon)$, by matching the wavefunctions of the wire Hamiltonian H_W between $j = N$ and $N + 1$,

$$\rho(\epsilon) = \frac{\sin(qa)\sin^2(ka)}{\pi a t[\sin^2(ka) + \frac{eV_g}{t} \sin[k(N+1)a] \sin(kNa)]}. \tag{3}$$

k and q are the wavevectors in $|x| < L$ and $|x| > L$, respectively, satisfying $\epsilon = \epsilon_0 - 2t\cos(ka) = \epsilon_0 - eV_g - 2t\cos(qa)$. For finite L, the hybridization function $\Gamma(\epsilon) = 2\pi t_{WD}^2 \rho(\epsilon)$ shows resonances with level spacing $\Delta \equiv \pi\hbar v_F/L$; see Fig. 2. The oscillation amplitude of $\Gamma(\epsilon)$ is proportional to V_g. The average value of $\Gamma(\epsilon)$ around ϵ_F is denoted as Γ_∞.

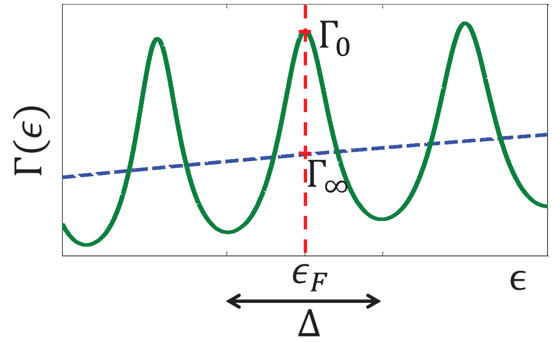

FIG. 2: (Color Online) Hybridization function $\Gamma(\epsilon) = 2\pi t_{WD}^2 \rho(\epsilon)$ for infinite (blue dashed curve) and finite L (green solid); we choose $\epsilon_0/2t = 0.931$ and $eV_g/2t = 0.125$. For finite L, $\Gamma(\epsilon)$ shows resonances with spacing $\Delta \equiv \pi\hbar v_F/L$; ϵ_F is chosen to be located at a resonance center (see the red dashed line). When L is so large that V_g is applied outside the Kondo cloud, the Kondo temperature $T_K = T_{K\infty}$ is determined by Γ_∞ and independent of V_g. On the other hand, T_K depends on V_g and L, when L is smaller than the cloud size ξ_K. When L is much smaller than ξ_K, T_K is determined by $\Gamma_0 \equiv \Gamma(\epsilon_F)$.

We sketch how the change of $\rho(\epsilon)$ by V_g affects the Kondo effect in different regimes of L. In the limit of $L \to \infty$, the Kondo temperature is determined by Γ_∞ as $T_{K\infty} \sim \sqrt{\Gamma_\infty U/2} \exp[\pi(\epsilon_d - \epsilon_F)(U + \epsilon_d - \epsilon_F)/(2\Gamma_\infty U)]$, and the cloud size is $\xi_{K\infty} = \hbar v_F/(k_B T_{K\infty})$. For $L \gg \xi_{K\infty}$ (i.e., $T_{K\infty} \gg \Delta$), many resonances of $\Gamma(\epsilon)$ around ϵ_F contribute to the Kondo effect, and their average value Γ_∞ results in $T_K = T_{K\infty}$. In this regime, the Kondo cloud is not sensitive to V_g. On the other hand, for $L \ll \xi_{K\infty}$ (i.e., $T_{K\infty} \ll \Delta$), the resonance of $\Gamma(\epsilon)$ located at ϵ_F, namely $\Gamma_0 \equiv \Gamma(\epsilon_F)$, mainly determines the Kondo effect, resulting in $T_K = T_{K0} \sim \sqrt{\Gamma_0 U/2} \exp[\pi(\epsilon_d - \epsilon_F)(U + \epsilon_d - \epsilon_F)/(2\Gamma_0 U)]$ and $\xi_K = \hbar v_F/(k_B T_{K0})$. In this case, V_g directly affects conduction electrons within the cloud, and modifies T_K.

Below, we will discuss the change of T_K between T_{K0} and $T_{K\infty}$ as a function of L/ξ_K in the two possible situations, case A where one changes L with keeping t_{WD} (hence $T_{K\infty}$ and $\xi_{K\infty}$) constant, and case B where one changes t_{WD} with keeping L constant.

Kondo temperature.— We compute the dependence of T_K on L and V_g analytically using the poor man scaling, and also numerically using the NRG approach [28].

In the poor man scaling, the renormalization of $J \to J + J^2(\int_{-D_0}^{-D} + \int_{D}^{D_0}) d\epsilon \rho(\epsilon)/|\epsilon|$ is performed with reducing the energy bandwidth of the wire from D_0 to D, and stopped at the bandwidth where $J^2 \int d\epsilon \rho(\epsilon)/|\epsilon|$ is comparable with J. The final bandwidth provides the scale of T_K. From this and Eq. (3), we obtain

$$\begin{aligned} \ln(\frac{T_K}{T_{K\infty}}) &\simeq -\frac{eV_g \cos(k_F(2L+a))}{2t\sin^2(k_F a)} \text{Ci}(\frac{2L}{\xi_K}), & (4) \\ &\simeq -\frac{eV_g}{2t\sin^2(k_F a)} \text{Ci}(\frac{2L}{\xi_K}) \quad \text{for } k_F = k_{F,n}, & (5) \end{aligned}$$

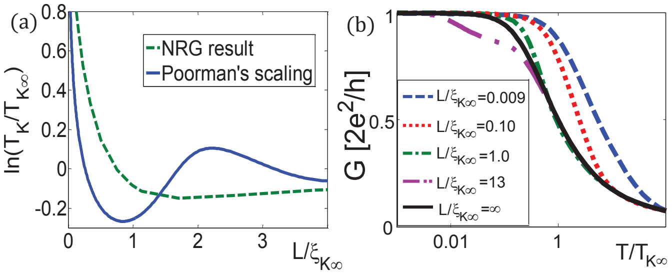

FIG. 3: (Color Online) Case A under the resonance condition of $k_F = k_{F,n}$. In this case, one changes L with keeping t_{WD} (hence $T_{K\infty}$ and $\xi_{K\infty}$) constant. (a) Kondo temperature T_K as a function of L, obtained by the poor man scaling (blue solid curve) and NRG (green dashed). The two approaches show qualitatively the same overall behavior that T_K drastically changes for $L \lesssim \xi_{K\infty}$, while $T_K \sim T_{K\infty}$ for $L \gtrsim \xi_{K\infty}$; their discrepancy in $L \gtrsim \xi_{K\infty}$ is discussed in the text. (b) NRG result of the temperature T dependence of conductance G for various values of $L/\xi_{K\infty}$. We choose $\Gamma_\infty/2t = 0.28$, $\epsilon_0/2t = 0.925$, $eV_g/2t = 0.125$, and $U/2t = 3.6$.

where $\text{Ci}(y) \equiv \int_{-\infty}^{-y} dy' (\cos y')/y'$, $k_{F,n} = 2\pi n/(2L+a)$, and n is an integer. Equation (4) is obtained by putting $k \to k_F \equiv k(\epsilon_F)$, $q \to q(\epsilon_F)$, $L \gg a$, $v_F \equiv \frac{1}{\hbar}\frac{\partial \epsilon}{\partial k}|_{k_F} = (2at/\hbar)\sin(k_F a)$, the small gate voltage of $|eV_g| \ll 2t\sin^2(k_F a)$, and the linearization of $\epsilon \simeq \epsilon_F + \hbar v_F (k - k_F)$ into Eq. (3); the simplication of $k \to k_F$ and $q \to q(\epsilon_F)$ is valid within the small energy scale of T_K. We remark that ξ_K depends on L and V_g in Eq. (4).

The dependence of T_K on L in Eq. (4) comes from the term $\text{Ci}(2L/\xi_K)$, which gives information on the cloud, and also from the $2k_F$ oscillation by the fact that the resonance centers in $\Gamma(\epsilon)$ shift across ϵ_F as L changes. One can focus on the former in the situations where the latter can be ignored. In case A, where one changes L, one can reduce the effect of the $2k_F$ oscillation, by tuning the system to a situation that ϵ_F is located near the bottom of an energy band (near the van Hove singularity) where the $2k_F$ term slowly oscillates, or by considering the resonance condition of $k_F = k_{F,n}$ where the $2k_F$ term provides the maximum value; see Eq. (5). The resonance condition can be achieved at each value of L, by tuning an additional gate voltage applied to the entire region of the wires (not shown in Fig. 1) with monitoring the conductance through the dot. On the other hand, in case B, the term $\cos(k_F(2L+a))$ is constant, hence can be ignored, since one changes t_{WD} with keeping L constant.

In case A under the resonance situation of $k_F = k_{F,n}$, the poor man scaling in Eq. (5) is plotted as a function of $L/\xi_{K\infty}$ (rather than L/ξ_K) in Fig. 3(a). As expected, T_K stays at $T_{K\infty}$ for $\xi_{K\infty} \lesssim L$, starts to drastically change around $L = \xi_{K\infty}$, and approaches to T_{K0} for $L \ll \xi_K$. This overall behavior is accompanied by the oscillation of $\ln(T_K/T_{K\infty}) \sim \text{sinc}(2L/\xi_{K\infty})$ for $L \gtrsim \xi_{K\infty}$, which is obtained from the asymptotic form of $\text{Ci}(x) \sim (\sin x)/x$ for $x \gg 1$ and by putting $\xi_K \simeq \xi_{K\infty}$ (valid for $L \gtrsim \xi_{K\infty}$) in Eq. (4). The sinc behavior originates from the average effect of the oscillation of $\rho(\epsilon)$ within $T_{K\infty}$; the average becomes more significant with increasing L, as the number $T_{K\infty}/\Delta$ of resonances within $T_{K\infty}$ increases. On the other hand, for $L \ll \xi_{K\infty}$, we find $\ln(T_K/T_{K\infty}) \propto -\ln(L/\xi_K)$, using $\text{Ci}(x) \sim \ln(x) + 0.577$ for $x \ll 1$. The above behavior of $T_K(L/\xi_{K\infty})$ reveals the Kondo cloud.

Conductance.— We compute the temperature T dependence of electron conductance G between the wires through the dot, by using the NRG approach [15, 26–28]. Below, we will discuss how to extract $\xi_{K\infty}$ from $G(T)$ in cases A (see Fig. 3) and B (Fig. 4).

We continue to discuss case A under the resonance condition of $k_F = k_{F,n}$. In Fig. 3(b), we plot $G(T)$ for different L's. It is custom [32] to get an estimate for T_K from the temperature at which $G(T)$ equals the half of the zero-temperature conductance of the $L \to \infty$ case. $G(T)$ shows the behavior distinct between $L \gtrsim \xi_{K\infty}$ and $L \lesssim \xi_{K\infty}$. For $L \gtrsim \xi_{K\infty}$, $G(T)$ equals to half of $G(T=0)$ of the $L \to \infty$ case at almost the same temperature, implying that T_K equals $T_{K\infty}$ independent of L in this regime. On the other hand, for $L \lesssim \xi_{K\infty}$, $G(T)$ shows that T_K changes toward T_{K0} as L decreases. This NRG result agrees with the poorman scaling; see Fig. 3(a). In this way, one directly measures $\xi_{K\infty}$.

There is a discrepancy between the two curves in Fig. 3(a). In the NRG case, $\ln(T_K/T_{K\infty})$ decreases only monotonously for $L \gtrsim \xi_K$, without showing the sinc behavior $\text{sinc}(2L/\xi_{K\infty})$ of the poor man scaling. The discrepancy may come from the known limitation that the logarithmic discretization scheme of NRG does not perfectly capture the behavior of high-energy states (higher than Δ in our case). On the other hand, for $L \ll \xi_{K\infty}$, where low-energy states mainly contribute to the Kondo effect, the NRG shows the same behavior of $\ln(T_K/T_{K\infty}) \sim -\ln(L/\xi_K)$ as the poorman scaling.

Next, we discuss case B where one changes t_{WD} with keeping L constant (hence $\Delta = \pi\hbar v_F/L$ does not alter). In Fig. 4, we plot the NRG result of $G(T)$ for different ξ_K's. In this case, one can obtain T_K from the high-temperature behavior of $G(T)$ in the same way as above, by choosing the temperature at which $G(T)$ equals the half of $G(T=0)$ of the $L \to \infty$ case. The result of T_K agrees with case A; see the inset of Fig. 4(b). We below suggest another way to see the cloud, based on the low-temperature behavior of $G(T)$. We note that as T changes across Δ, $G(T)$ can show a jump due to the resonance structure of $\rho(\epsilon)$, as shown in the case of $L/\xi_K = 26$ in Fig. 4(a).

We describe the regime of $T \ll T_K, \Delta$, using the fixed-point Hamiltonian of the Fermi liquid theory [6, 29, 33],

$$H_{\text{low}} \simeq \sum_{k\sigma} \epsilon_k c^\dagger_{k\sigma} c_{k\sigma} - \frac{1}{\pi\rho(\epsilon_F)} \sum_{kk'\sigma} \left(\frac{\epsilon_k + \epsilon_{k'}}{2T_K} + \delta_p\right) c^\dagger_{k\sigma} c_{k'\sigma} + \frac{1}{\pi T_K \rho^2(\epsilon_F)} \sum_{k_1 k_2 k_3 k_4} c^\dagger_{k_1\uparrow} c_{k_2\uparrow} c^\dagger_{k_3\downarrow} c_{k_4\downarrow}, \qquad (6)$$

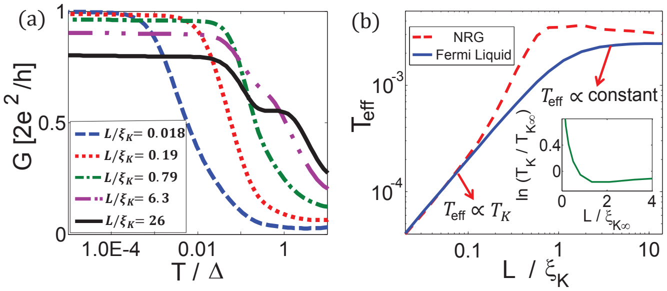

FIG. 4: (Color Online) Case B. In this case, one changes t_{WD} (hence ξ_K) with keeping L constant. (a) The NRG result of $G(T)$ for different values of t_{WD}; we show the values of ξ_K instead of t_{WD}. (b) $T_{\rm eff}$ [defined in Eq. (8)] as a function of L/ξ_K, obtained from the two different approaches of the Fermi liquid theory and the NRG. Inset: The NRG result of $T_K(L/\xi_{K\infty})$ exhibits the same behavior as Fig. 3(a). We choose $L = 100a$, $\epsilon_0/2t = 0.931$, $eV_g/2t = 0.125$, and $U/2t = 3.6$. ϵ_F is chosen to be located at the center of a resonance of $\Gamma(\epsilon)$, for simplicity.

where $c^\dagger_{k\sigma}$ creates an electron with momentum k, spin σ, and energy ϵ_k, and δ_p is the phase shift coming from the potential scattering (i.e. from the particle-hole symmetry breaking). Although ρ depends on ϵ, we take for simplicity a constant ρ in Eq. (6) as a crude approximation. The second term of Eq. (6) describes elastic scattering of electrons by the Kondo singlet, with scattering phase shift $\delta(\epsilon) = \pi/2 + (\epsilon - \epsilon_F)/T_K + \delta_p$. The third term shows repulsive interactions between quasiparticles that break the Kondo singlet, and contributes to inelastic T-matrix $t^{\rm in}$ as $-\pi\rho(\epsilon_F){\rm Im}t^{\rm in}(\epsilon) = [(\epsilon - \epsilon_F)^2 + \pi^2T^2]/(2T_K^2)$. By combining $\delta(\epsilon)$ and ${\rm Im}t^{\rm in}(\epsilon)$, one can obtain $G(T)$, following Ref. [6], as

$$G(T) = \frac{2e^2}{h}\frac{1+\cos(2\delta_p)}{2}\left(1 - \frac{\pi^2T^2}{T_{\rm eff}^2}\right), \qquad (7)$$

$$\frac{1}{T_{\rm eff}^2} \equiv \frac{2\beta}{3(\alpha+\beta)\Delta^2} + \frac{2\cos(2\delta_p)}{(1+\cos(2\delta_p))T_K^2}, \qquad (8)$$

where α and β are constants depending on V_g and k_F but independent of L. δ_p is obtained by comparing $G(T = 0)$ with Eq. (7). When δ_p is nonzero (i.e., when the particle-hole symmetry is broken), the potential scattering contributes to $G(T)$, causing the deviation of $G(T = 0)$ from the unitary-limit value of $2e^2/h$. Note that when ρ is independent of ϵ and the particle-hole symmetry is preserved, $\delta_p = 0$ and $\beta = 0$, hence, $T_{\rm eff} \to T_K$.

$T_{\rm eff}$ is obtained by comparing $G(T)$ with Eq. (7) in experiments or in the NRG approach, while it is directly computed from Eq. (8) in the Fermi liquid theory. We plot $T_{\rm eff}(L/\xi_K)$ in Fig. 4(b), which shows that the NRG and the Fermi liquid theory are in good agreement; their quantitative discrepancy may come from the approximation in our Fermi liquid theory mentioned above.

The dependence of $T_{\rm eff}$ on L/ξ_K or $L/\xi_{K\infty}$ is useful for identifying ξ_K in case B, since Δ is constant so that $T_{\rm eff}(L/\xi_K)$ directly provides the information of $T_K(L/\xi_K)$; see Eq. (8). For $L \gtrsim \xi_K$, $T_{\rm eff}$ is almost constant, implying that T_K and ξ_K are independent of L. For $L \lesssim \xi_K$, $T_{\rm eff}$ (hence T_K) depends on L/ξ_K. The crossover occurs around $\xi_K \simeq L$, providing a direct evidence of the cloud.

Conclusion.— In this Letter we proposed a way to directly detect, by electrical means, the Kondo cloud, based on the competition between the cloud length and the distance between the Kondo impurity and the region of conduction electrons to which a gate voltage is applied.

Our proposal may be within experimental reach. Case A, where L varies, may be achieved with keyboard-type gate voltages, while one easily tunes t_{WD} in case B. For both the cases, the wire whose Fermi level is located near the bottom (van Hove singularity) of an energy band is useful to achieve a conclusive evidence of the cloud. Near the van Hove singularity, $\rho(\epsilon)$ is sensitive to V_g, resulting in large difference between $T_{K\infty}$ and T_{K0}. Moreover, near the van Hove singularity, the Fermi wave length $1/k_F \gg L, \xi_K$; hence we expect that the $2k_F$ term in Eq. (4) will oscillate slowly as a function of L in the regime of L where the transition between $T_{K\infty}$ and T_{K0} occurs. If we assume that in this limit $1/k_F$ is also longer than the length scale over which $V_g(x)$ spatially changes at $x = L$, we expect that then the $2k_F$ oscillations will not be washed out. A good candidate for our proposal may be a carbon nanotube, where one expects $T_K \sim 1$ K and ξ_K of a micrometer [34].

We thank I. Affleck, G. Finkelstein, L. Glazman, D. Goldharber-Gordon, S. Ilani, A. K. Mitchell, S. Tarucha for useful discussions, and Minchul Lee for advices on NRG calculations. We acknowledge support by NRF (grant 2011-0022955; HSS), and by BSF and Minerva grants (YO). HSS thanks J. Moore and UC Berkeley, where this paper is written, for hospitality.

---

[*] Electronic address: hssim@kaist.ac.kr

[1] J. Kondo, Prog. Theor. Phys. **32**, 37 (1964).
[2] A. C. Hewson, *The Kondo Problem to Heavy Fermions* (Cambridge University Press, Cambridge, 1993).
[3] D. Goldhaber-Gordon *et al.*, Nature (London) 391, 156 (1998).
[4] S. M. Cronenwett, T. H. Oosterkamp, and L. P. Kouwenhoven, Science **281**, 540 (1998).
[5] L. Kouwenhoven and L. I. Glazman, Physics World **14**, 33 (2001).
[6] L. I. Glazman and M. Pustilnik, in *Nanophysics: Coherence and Transport*, eds. H. Bouchiat *et al.* (Elsevier, 2005), pp. 427-478.
[7] J. E. Gubernatis, J. E. Hirsch, and D. J. Scalapino, Phys. Rev. B **35**, 8478 (1987).
[8] V. Barzykin and I. Affleck, Phys. Rev. Lett. **76** 4959, (1996); Phys. Rev. B **57**, 432 (1998).
[9] L. Borda, Phys. Rev. B **75**, 041307 (2007).

[10] A. Holzner *et. al*, Phys. Rev. B **80**, 205114 (2009).
[11] I. Affleck, L. Borda, and H. Saleur, Phys. Rev. B **77**, 180404 (2008).
[12] C. A. Büsser *et al.*, Phys. Rev. B **81**, 045111 (2010).
[13] A. K. Mitchell, M. Becker, and R. Bulla, Phys. Rev. B **84** 115120 (2011).
[14] I. Affleck and P. Simon, Phys. Rev. Lett. **86**, 2854 (2001).
[15] P. S. Cornaglia and C. A. Balseiro, Phys. Rev. B **66**, 115303 (2002); Phys, Rev. Lett. **90**, 216801 (2003).
[16] P. Simon and I. Affleck, Phys. Rev. Lett. **89**, 206602 (2002); Phys. Rev. B **68**, 115304 (2003).
[17] T. Hand, J. Kroha, and H. Monien, Phys. Rev. Lett. **97**, 136604 (2006).
[18] R. Yoshii and M. Eto, Phys. Rev. B **83** 165310 (2011).
[19] E. S. Sϕrensen and I. Affleck, Phys. Rev. B **53**, 9153 (2005).
[20] For a review, see I. Affleck, in *Perspectives of Mesoscopic Physics* (World Scientific, 2010), pp. 1-44.
[21] J. P. Boyce and C. P. Slichter, Phys. Rev. Lett. **32**, 61 (1974); Phys. Rev. B **13**, 379 (1976).
[22] V. Madhavan *et al.*, Science **280**, 567 (1998).
[23] H. C. Manoharan, C. P. Lutz, and D. M. Eigler, Nature **403**, 512 (2000).
[24] H. Prüser *et al.* Nat. Phys. **7**, 203 (2011).
[25] P. W. Anderson, J. Phys. C **3**, 2439 (1970).
[26] K. G. Wilson, Rev. Mod. Phys. **47**, 773 (1975); H. R. Krishna-murthy, J. W. Wilkins, and K. G. Wilson, Phys. Rev. B **21**, 1003 (1980).
[27] R. Bulla, T. A. Costi, and T. Pruschke, Rev. Mod. Phys. **80**, 395 (2008).
[28] We use the full desnity matrix NRG method developed by A. Weichselbaum and J. von Delft, Phys. Rev. Lett. **99**, 076402 (2007). We use the NRG discretization parameter of $\Lambda = 2$ and keep ~ 300 states at each iteration.
[29] P. Nozières, J. Low Temp. Phys. **17**, 31 (1974); J. Phys. (Paris) **39**, 1117 (1978).
[30] P. W. Anderson, Phys. Rev. **124**, 41 (1961).
[31] J. R. Schrieffer and P. A. Wolff, Phys. Rev. **149**, 491 (1966).
[32] D. Goldhaber-Gordon *et al.*, Phys. Rev. Lett. **81**, 5225 (1998).
[33] I. Affleck and A. W. W. Ludwig, Phys. Rev. B **48**, 7297 (1993).
[34] J. Nygard, D. H. Cobden, and P. E. Lindelof, Nature **408**, 342 (2000).